Experimental study of hydrogen plasma breakdown in a 2.45 GHz microwave discharge

Experimental study of hydrogen plasma breakdown in a 2.45 GHz microwave discharge

O D Cortázar[1,2]**, J Komppula**[3]**, O Tarvainen**[3]**, A Megía-Macías**[1]**,**
A Vizcaíno-de-Julián[1] **and H Koivisto**[3]

[1] ESS Bilbao Consortium, Edificio Cosimet, Landabarri 2, Planta 1, 48940-Leioa, Vizcaya, Spain
[2] Applied Mechanics and Engineering Projects Department, University of Castilla-La Mancha, ETSII,
c/ Camilo Jose Cela s/n, 13071-Ciudad Real, Spain
[3] Department of Physics, University of Jyväskylä, PO Box 35 (YFL), 40500 Jyväskylä, Finland

E-mail: dcortazar@essbilbao.org

Abstract
Temporal evolution of microwave-plasma coupling, vacuum ultraviolet (VUV) light emission
and plasma electron temperature and density is reported for a 2.45 GHz microwave hydrogen
discharge pulsed at 50 Hz. Directional couplers, a VUV spectrometer and a Langmuir probe
are used for the diagnostics of the plasma breakdown. A 5–10 μs transient peak of light
emission exceeding the steady-state intensity by a factor of 3.3 is observed in coincidence with
an abrupt drop in the microwave electric field. Observed light emission intensities combined
with cross section data indicate that the electron temperature during the breakdown transient
exceeds the steady-state value of 4–6 eV by a factor $\geqslant 3$, which is in good agreement with the
Langmuir probe data. The estimated magnitude of the electron temperature transient
corresponds well with the microwave-plasma coupling characteristics, indicating a drop of
30–40% in the electric field strength due to plasma damping.

(Some figures may appear in colour only in the online journal)

1. Introduction

Transient effects in pulsed electron cyclotron resonance (ECR) discharges are of high interest for applications, e.g. particle accelerators and the plasma processing industry [1, 2]. Research on this subject has been conducted mainly with high-frequency minimum-B ECR ion sources by different researchers using electrical probes, spectroscopy and radiation diagnostics under a wide range of parameters for different plasmas [3–10]. The research on 2.45 GHz microwave hydrogen ion sources has been, to a great extent, focused on studying the temporal properties of extracted ion beams such as species fraction [11] and the effect of pulse pattern on the horizontal beam emittance [12]. Temporally and spatially resolved Langmuir probe diagnostics for pulse-modulated hydrogen discharges in planar microwave plasma reactors at 2.45 GHz have been published recently by Rousseau *et al* [13] reporting a temperature peak at the beginning of the discharge pulse.

In this paper, we present an experimental study of plasma breakdown in hydrogen discharges of a 2.45 GHz microwave plasma generator developed to study ECR plasmas with the aim of improving ECR ion sources. The diagnostic setup makes use of several complementary techniques, i.e. directional couplers for incident and reflected power measurements, a vacuum-ultraviolet (VUV) spectrometer and a Langmuir probe providing data with μs-level temporal resolution. These diagnostic methods provide data related to the transient phenomena in fundamentally different ways. The incident and reflected power sensors provide information on the interaction between the electromagnetic waves and the plasma, which depends mainly on the plasma density and absorption efficiency of the energy carried by the microwave. VUV light emission is a consequence of the interaction between energetic (>10 eV) electrons and neutrals in excitation reactions. On the other hand, VUV-emission signal can be considered as a measure of the ionization rate because the ratio of the excitation and ionization cross sections for hydrogen is
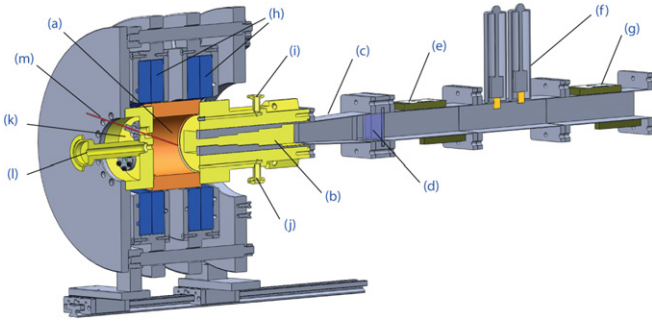
Figure 1. A view of plasma reactor and its main subsystems: (*a*) plasma chamber; (*b*) ridged waveguide; (*c*) waveguide adapter; (*d*) quartz window; (*e*) dual directional coupler for synchronization signal; (*f*) two-stub tuner; (*g*) dual directional coupler for measuring incoming and reflected power; (*h*) coil pancakes; (*i*) gas inlet; (*j*) pressure gauge inlet; (*k*) diagnostic port; (*l*) pumped and line-of-sight for optical diagnostics; (*m*) tilted Langmuir probe.

Figure 2. Photograph of the experimental setup. The VUV spectrometer on the left is connected to the plasma generator on the right.

well defined [14]. The Langmuir probe is sensitive to all electromagnetic properties of the plasma, e.g. plasma potential, external magnetic field and charged particle energy and density. Langmuir probe diagnostics of the given setup have been reported recently in [15]. Since Langmuir probe diagnostics are known to be somewhat sensitive to the chosen analysis method, external magnetic field and exact nature of the electron energy distribution, as discussed thoroughly by Chen *et al* in [16], we have used the complementary diagnostic setup described in this paper to confirm that the average energy of the electrons peaks during the plasma breakdown transient. In this study we focus on a single experimental condition to describe the interpretation of the data. However, additional data obtained through the VUV diagnostics are presented to demonstrate that the conclusions are valid over a wide range of experimental conditions. This study is intended to broaden the understanding of the plasma breakdown dynamics of ECR plasmas. In particular, it reveals similarities of the plasma breakdown transient effects observed earlier with high-frequency ECR ion sources intended for the production of multicharged ions and 2.45 GHz microwave discharges often used for the production of high-current monocharged ion beams. Also, to put our research into a wider context, it is worth noting that the observed transient effects take place on μs scale and, thus, are interpreted to originate from the temporal evolution of the electron energy distribution rather than neutral gas heating and subsequent depletion, often observed in various plasma generators, as first discussed by Boswell [17].

## 2. Experimental setup and procedure

The experiments were conducted with a plasma generator driven by a 2.45 GHz/3 kW adjustable power magnetron pulsed at 50 Hz. The plasma generator is shown in figure 1 with the main subsystems. The device is a reproduction of the ISHP (Ion Source of Hydrogen Positive) ion source under development at ESS Bilbao with the exception of the plasma electrode and extraction being replaced by an optical diagnostic port. The plasma chamber (*a*) is cylindrical with 93 mm
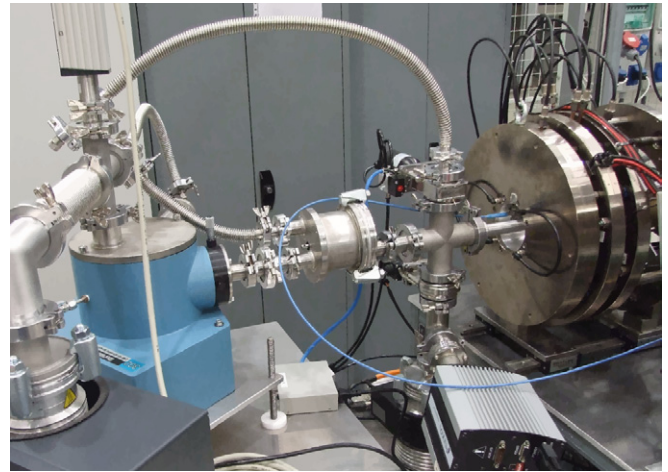
length by 90 mm diameter and is made of OFHC copper including an external water cooling bath for heat removal. Microwave radiation is coupled into the plasma chamber through a ridged waveguide section of 280 mm length with a WR284 waveguide input connection (*b*). A WR284–WR340 adaptor of 128 mm length (*c*) connects the ridged waveguide piece with a 30 mm long window holder, which houses a 10 mm thick rectangular quartz window vacuum break (*d*). The parts at atmospheric pressure include a dual directional coupler (*e*) that is used to obtain timing synchronization signals, a two-stub tuner (*f*) for fine-tuning of the impedance matching and another dual directional coupler (*g*) where incoming and reflected power from the magnetron and the plasma are measured. Each of these three sections (*e*–*g*) is 173 mm in length. The 2.45 GHz/3 kW magnetron (model MH3000s-213BB by MUEGGE company, not shown in the figure) is connected to the directional coupler (*g*) through a 610 mm long straight waveguide. The emission head of the magnetron is protected from the reflected power by a water cooled circulator, which also effectively mitigates the frequency variation due to varying load impedance. Four coaxial coils (*h*) arranged in two pancakes are excited independently to produce different impressed magnetic field profiles. The topology and strength of the magnetic field can be adjusted by tuning the coil currents and positioning the coil pancakes. Hydrogen is injected into the plasma chamber through a needle valve in the gas inlet (*i*). The gas feed rate is measured by a digital flow meter and pressure by a gauge connected to the plasma chamber (*j*). Both sides of the plasma chamber are covered by 2 mm thick boron nitride disks properly machined to fit the microwave port, gas inlet and diagnostic portholes. The downstream end of the plasma chamber (*k*) is used for pumping and diagnostics including an axial line-of-sight for optical diagnostics (*l*) and tilted feedthrough for the Langmuir probe (*m*), the latter being retrofitted for the present experiments.

A view of the experimental setup is shown in figure 2, where the UVV spectrometer can be seen on the left-hand side and the plasma chamber surrounded by the coil pancakes on the right. Figure 3 shows a schematic of the diagnostics and
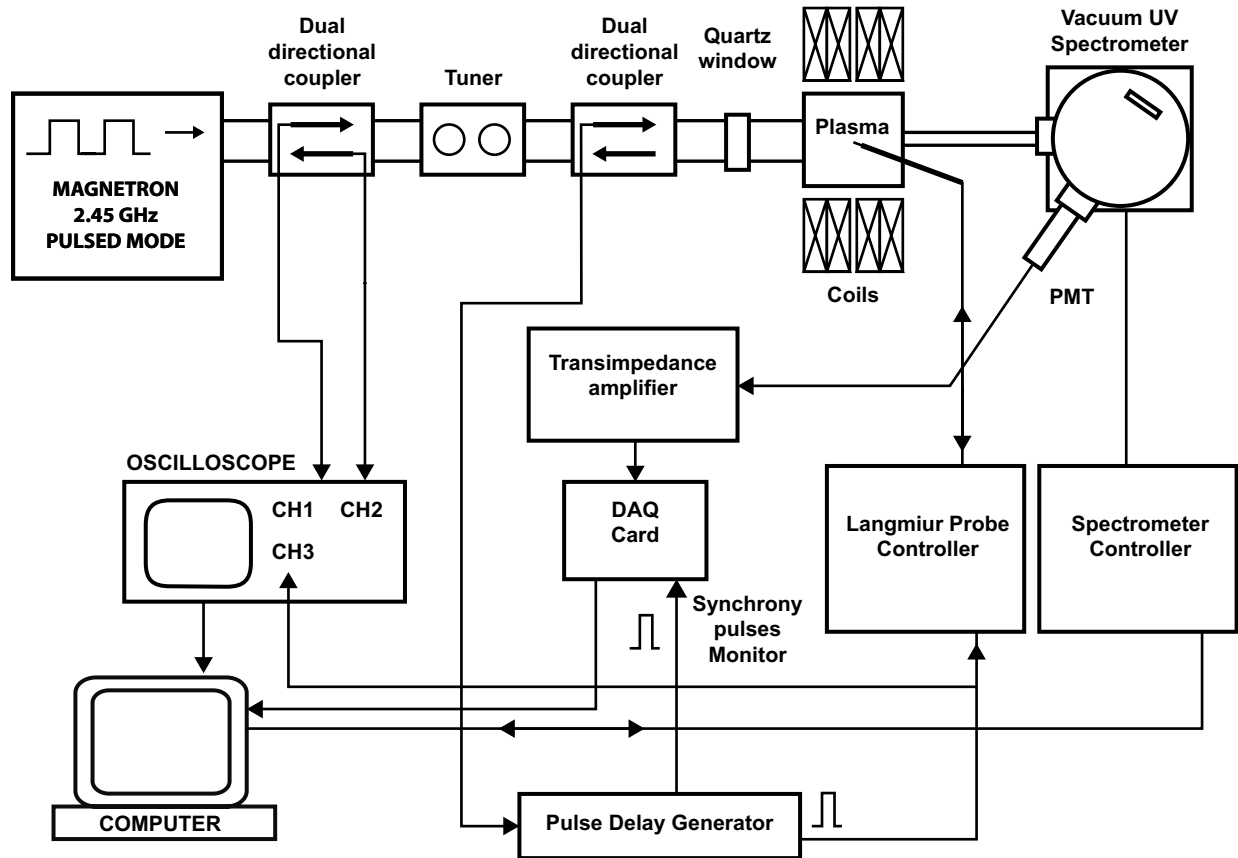
Figure 3. Schematic presentation of the diagnostic setup for measuring the temporal evolution of microwave-plasma coupling, VUV light emission and plasma electron temperature and density.

timing system integrated to the plasma reactor. The timing signal for data acquisition, provided by the dual directional coupler, is used for triggering the VUV diagnostics as well as the Langmuir probe via a delay generator. The positions of the tuner stubs are adjusted in order to obtain the minimum reflected power readout corresponding to a stable plasma and low jitter between the timing signals for consecutive microwave pulses (jitter is always kept below $0.1\,\mu$s). Both dual directional couplers have a 60 dB coupling factor with an approximated coupling loss of 4×10^{-6} dB and a directivity of 25 dB. The VUV spectrometer consists of a monochromator (McPherson, model 302) equipped with a holographic grating, a photomultiplier tube (PMT, ET Enterprises, model 9406B) and PC controlling the wavelength in the range 100–250 nm. A transimpedance amplifier connected to the NI USB-6255 data acquisition card, triggered by the falling edge of the reflected power signal associated with the plasma breakdown, is used for recording the photomultiplier current. The spectral and temporal resolutions of the VUV spectrometer were 9 nm—set to this value with slits to increase the light intensity at the PMT—and $2\,\mu$s, respectively. In order to reduce noise, 100 consecutive pulses are recorded and averaged, which translates to data acquisition time of a few seconds for the VUV light. VUV diagnostics are favored over the less complicated visible line diagnostics because excitation cross sections to the first excited states of atoms and molecules are an order of magnitude higher than the

excitation cross sections to the higher states, e.g. Balmer series and Fulcher band [14]. Also the excitation energy is lower, which means that the excitation rate is less sensitive to the changes of the tail of the electron energy distribution function (EEDF), which is especially important when studying transient effects. Measuring molecular emission within the Lyman band ($\sim$161 nm) is probably the best diagnostics tool of the excitation rate because the given transitions do not suffer significantly from cascade effects from higher excited states [18].

The Langmuir probe is used for acquiring I–V curves permitting one to estimate the plasma electron temperature and density. The probe tip is made of a 6 mm long and 0.5 mm diameter tungsten wire. Transient effects are studied by synchronizing the probe with the VUV-emission measurement via a delay generator and building the I–V curve from the data obtained over consecutive pulses. The Langmuir probe driver circuit (ESPION) is made by Hiden Analytical LTD and it acquires a single I–V point in 62.5 ns and rearms itself in another $14.6\,\mu$s required for data handling. Each point of the I–V curve is an average of the probe currents acquired over 100 consecutive pulses at a fixed probe voltage. Altogether it takes several minutes to acquire a complete I–V curve corresponding to a single temporal data point, which inevitably exposes the measurement and data analysis to long-term shifts in plasma conditions and pulse-to-pulse oscillations. These effects can be minimized by careful tuning of the microwave coupling and averaging of the data.
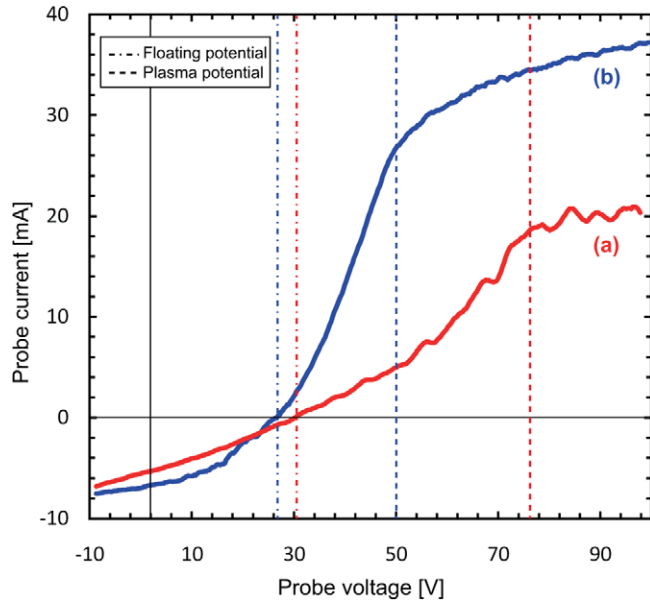
Figure 4. Langmuir probe $I-V$ curves obtained during the experiments. Curve (*a*): typical case corresponding to the breakdown. Curve (*b*): typical case during the steady-state plasma condition (15 and 60 μs after incoming microwave pulse). Floating potential and plasma potential are indicated by dotted vertical lines.

The electron temperature T_e is estimated from the $I-V$ curve assuming a Maxwellian EEDF [19, 20]. T_e values are also estimated from the difference of plasma potential and floating, potential, i.e. $V_p - V_f = (kT_e/2) \ln (2m_i/\pi m_e)$, where kT_e is in units of eV [16, 21]. For hydrogen plasmas with varying species fraction this translates to $T_e = 0.26...0.28(V_p - V_f)$. It is plausible that the external magnetic field increases the coefficient to values > 0.3 [16] but due to the tilt of the probe it is impossible to arrive at a precise estimate. Thus, we have used the coefficient of 0.26, which corresponds to the minimum (theoretical) value for T_e and assumes a perfectly Maxwellian EEDF. Deriving the error directly from the measured quantities is almost impossible since commonly accepted probe analysis techniques are not always supported by theory and include assumptions [16, 19, 20]. Figure 4 shows typical $I-V$ curves obtained during the experiments. Curve (a) is measured at 15 μs, i.e. during the plasma breakdown transient discussed in the following section and curve (b) at 60 μs, i.e. after reaching the steady state. The plasma potential is determined by taking the derivative of the $I-V$-curve and using half of its maximum value as a criterion for the 'knee'. The shape of the curve is defined by the EEDF as well as sheath expansion at high probe voltages [19, 21]. The orientation (tilt) of the probe with respect to the external magnetic field results in slight underestimation of the saturation currents since the electron Larmor radius is smaller than the diameter of the probe tip causing the field lines intercepting the probe to become partially depleted due to the limited diffusion rate across the field [21]. The shape of the curve suggests that the plasma density is always below the critical density, i.e. 7.44×10^{16} m^{-3} for 2.45 GHz microwaves. The plasma density of the given plasma generator has been estimated previously by modeling the ion saturation branch of the $I-V$ curve based on numerical results by Laframboise [15, 20].

In the experiments reported here the plasma breakdown transient was studied keeping the repetition rate (50 Hz) and duty cycle (50%) fixed while varying the microwave power from 300 to 3000 W and neutral hydrogen pressure from 3.8 to 9.3×10^{-3} mbar. The experimental conditions are typical for microwave discharge ion sources intended for proton beam production (see, e.g., [22]). Figure 5 shows a 2D cross-sectional view of the magnetic field profile corresponding to the experimental condition described in detail in the following section. The given profile, simulated with FEMM 4.2 [23] and validated by measurements, results in low reflected power, and short and reproducible microwave coupling time [24]. The plasma chamber boundaries are represented by the rectangular shape defined by the solid black line where the left-hand side corresponds to the microwave injection side and the right-hand side side to the diagnostic port. A dotted black line indicates the position of the 87.5 mT ECR surface. The magnetic field at the Langmuir probe position ($r = 0$, $z = 46.5$ mm) is about 120 mT. Probe data were taken at 1 μs interval during the ignition transient, followed by gradual increase of the time step to 20 μs after reaching the steady state.

3. Experimental results and discussion

Figure 6 shows a typical result for the temporal evolution of the measured parameters. The corresponding settings are 900 W incident power, 9.3×10^{-3} mbar hydrogen pressure and magnetic field profile depicted in figure 5. The reflected-to-incident power ratio P_r/P_i is shown in figure 6(a). First, the power absorption is poor, allowing the electric field strength in the plasma chamber to reach a value characteristic for the coupling system and cavity. The P_r/P_i ratio can be used for calculating the relative change of the average microwave electric field in the plasma chamber as a function of time from [6, 25]

$$\frac{E(t)}{E_{max}} = \sqrt{\frac{\left(1 \mp \sqrt{R(t)}\right)\left(1 \pm \sqrt{R_{max}}\right)}{\left(1 \pm \sqrt{R(t)}\right)\left(1 \mp \sqrt{R_{max}}\right)} \frac{(1 - R(t))}{(1 - R_{max})}} \quad (1)$$

where $R = P_r/P_i$ and negative/positive sign corresponds to under-overcoupled cavity. The result displayed in figure 6(a) is normalized to the maximum field, corresponding to R_{max} where $\sim$10% of the power is lost in transmission, e.g. in the waveguide. Because the system is not designed for any eigenmode and has a small radius-to-wavelength ratio of 0.36, it is further assumed that the cavity is undercoupled. The calculation suggests that the electric field drops to $\sim$60% of the unloaded value during the plasma breakdown. This represents the upper limit for the average electric field since the plasma refractive index has been assumed to be equal to its incident value in vacuum, i.e. unity, which causes an estimated error of 10% in steady state. The relatively modest drop of the electric field is explained by a low Q-value of the cavity. The calculation of the average electric field from equation (1) is based on the properties of microwave-plasma coupling, not on modeling the actual electron heating mechanism or the actual electric field pattern that shifts during the breakdown in an unknown manner. In order to gain confidence on the result
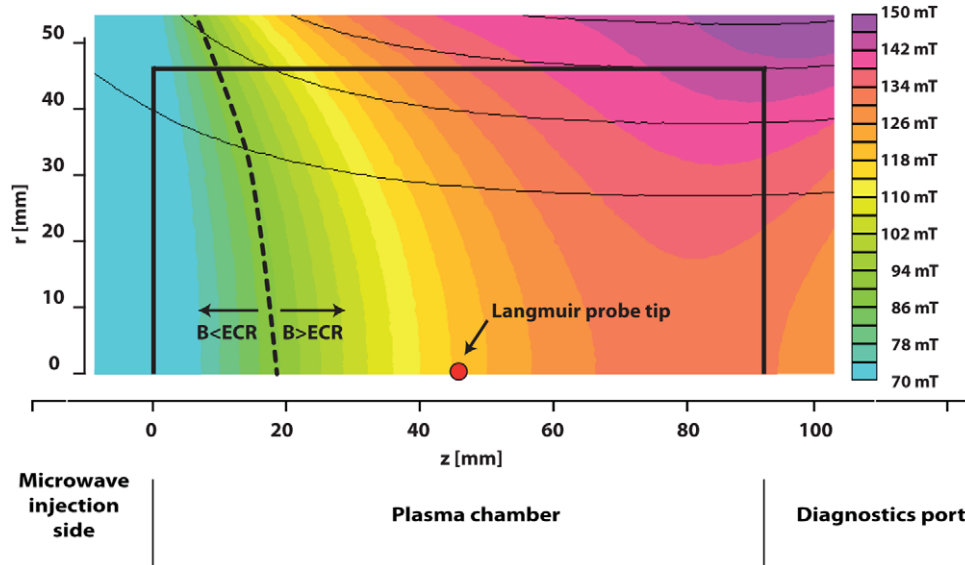
Figure 5. 2D cross section of the magnetic field configuration used in the experiments. The plasma chamber is represented by a black solid line. The dotted black line indicates the position of the ECR surface (87.5 mT).

another approach based on [26], where the electron heating at the ECR zone is studied theoretically, is presented. Due to the long wavelength it can be assumed that the incident microwave power is either reflected or absorbed, i.e. $P_i = P_r + P_a$. The absorbed power P_a consists of the fraction absorbed by the plasma and transmission losses, P_{loss}. Following [26] the ratio of the 'effective electric field' to the incident electric field can be expressed as

$$\frac{E_{\text{eff}}(t)}{E_{\text{max}}} = \sqrt{\frac{(P_r + P_{\text{loss}})/P_i - 1}{\ln\left(\frac{P_r + P_{\text{loss}}}{P_i}\right)}}. \quad (2)$$

The measured ratio of reflected-to-incident power at the beginning of the microwave pulse is about 90% indicating that transmission losses account for 10% of the incident power. The temporal evolution of the electric field calculated from equation (2) is also shown in figure 6(a). The result suggests that the electric field drops to ∼65% of the initial value due to plasma damping. Thus, the results calculated with the alternative models are in reasonable agreement. The temporal evolution of VUV light emission at 160 nm, i.e. at the maximum of molecular Lyman band extending from 125 to 161 nm, and at 121.6 nm corresponding to the Lyman-α transition is presented in figure 6(b). Lyman band transitions $\left(B\,^1\Sigma_g^+ \rightarrow X\,^1\Sigma_u^+\right)$ are caused by electron impact on excited neutral hydrogen molecules (e + H$_2$ $\rightarrow$ Lyman band). Since electron losses are dominated by diffusion, the rate of recombination reactions resulting in Lyman band emission is insignificant in comparison with electron impact excitation [27]. Lyman-α corresponds to the electronic transition of hydrogen atom from the first excited state to the ground state ($n = 2 \rightarrow n = 1$). The transient peak of light emission lasting some μs is observed in coincidence with the drop in the electric field. After the ignition transient, the Lyman band and Lyman-α emission intensities exhibit opposite trends,

i.e. molecular/atomic emission decreases/increases slowly and saturates at ∼500 μs.
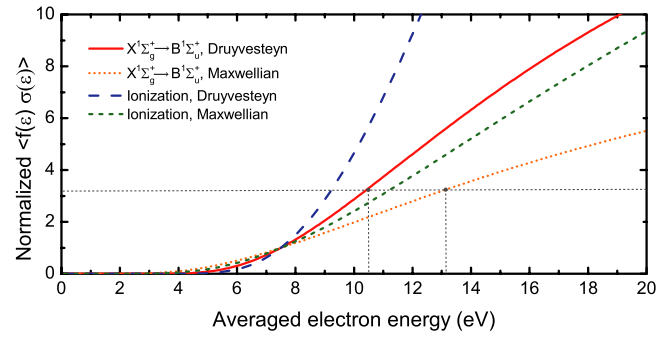
Figure 6(c) shows the temporal evolution of the floating potential and plasma potential, determined from the zero-crossing of the (averaged) I–V curve and the 'knee' of the curve, as described previously. It is evident from the data that both potentials fluctuate during the breakdown process which increases the uncertainty of the probe analysis in comparison with the steady state. Figure 6(d) shows the temporal evolution of electron temperature obtained with two analytical methods, i.e. with the Laframboise method (used in [15]) and from the difference of the aforementioned potentials. Altogether, the probe data indicate the existence of a breakdown transient before the temperature saturates to about 4–6 eV at about 20–50 μs and remains at this level until the end of the microwave pulse. The temporal evolution of the electron saturation current (defined at $V_{\text{probe}} = V_{\text{plasma}}$) is presented in figure 6(e). The electron current at the 'knee' of the I–V curve reflects the plasma density, which is therefore interpreted to increase monotonically up to 20 μs, which is equal to the time it takes for the average electric field to collapse. The volumetric rate of ionizing collisions is proportional to the electron and neutral gas densities and ionization rate. Thus, it is expected that the electron density first increases exponentially and then saturates to a level where loss rate of electrons due to diffusion and recombination equals the ionization rate of the neutral gas, which agrees well with the data in the P_r/P_i ratio and average electric field is caused by the presence of electrons absorbing the microwave power and damping the microwave EM field. A similar effect on the microwave-plasma coupling has been observed with high-frequency ECR ion sources [6, 28] but has never been directly correlated with the temporal evolution of the plasma density.

Figure 7 shows the rates for ionization and excitation of H$_2$ molecules as a function of electron average energy for Maxwell–Boltzmann and Druyvesteyn EEDFs, which is considered more representative for plasmas where

5
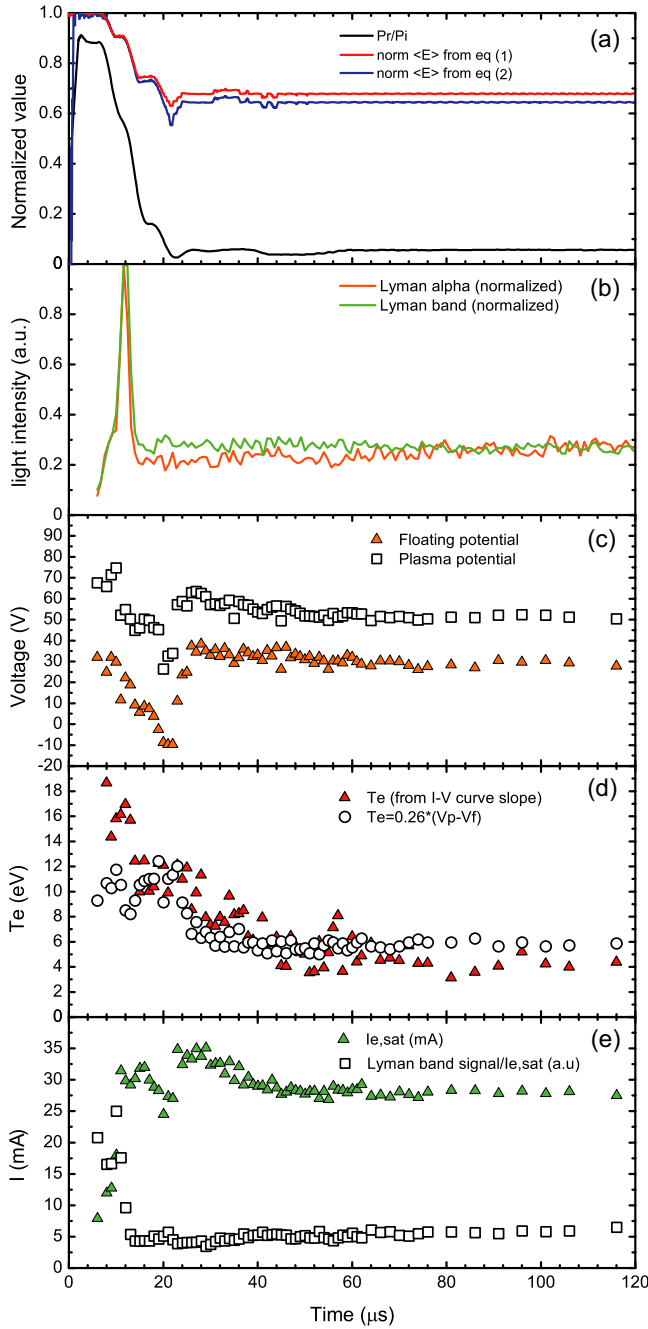
Figure 6. Time-resolved signals and plasma parameters during the breakdown of a hydrogen discharge in a 2.45 GHz plasma generator. (*a*) P_r/P_i and average electric field, (*b*) Lyman band and Lyman-α VUV light emission, (*c*) floating and plasma potential, (*d*) electron temperature by two different methods, (*e*) saturation electron current and the ratio between Lyman band emission signal and saturation electron current.

Figure 7. Normalized rates of ionization and molecular excitation resulting in Lyman band emission for hydrogen as a function of average electron energy.
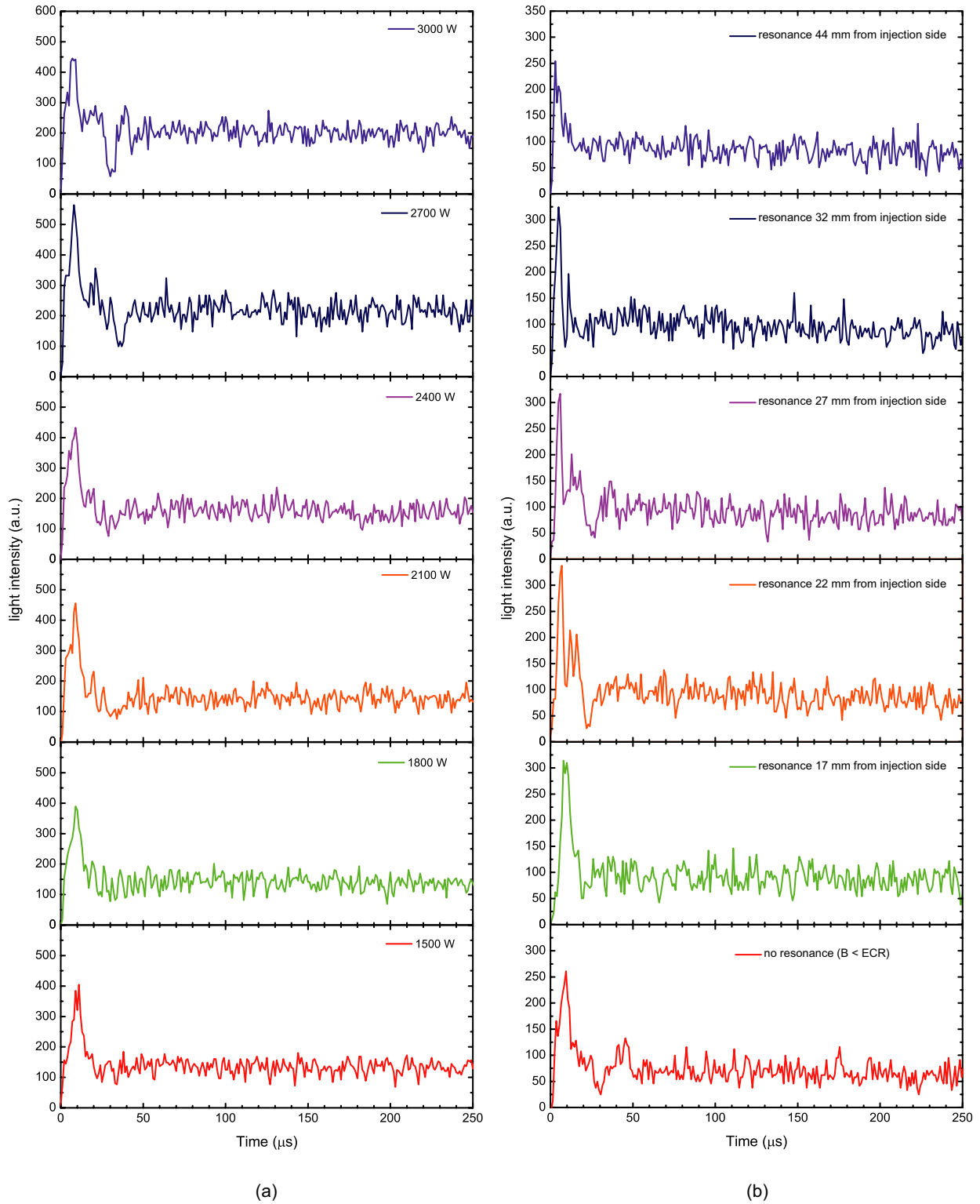
of the probe sheath, which is considered to be constant for $V_{\text{probe}} < V_{\text{p}}$. The average electron velocity v_e is proportional to the square root of the average electron energy, i.e. $E^{0.5}$. Thus, $I_{e,\text{sat}} \sim n_e \langle E \rangle^{0.5}$. On the other hand, the Lyman band emission signal is proportional to the electron density and the molecular excitation rate, the latter being proportional to $\langle E \rangle^x$, where $x > 1$, as shown in figure 7. Dividing the Lyman band VUV signal by the electron saturation current yields a quantity that is proportional to $\langle E \rangle^y$, where $y > 0.5$ (the plasma density dependence cancel each other). The peak of the Lyman band signal/$I_{e,\text{sat}}$ ratio in figure 6(*e*) is therefore interpreted as evidence of electron average energy (or temperature) peaking during the plasma breakdown transient.

The intensity of Lyman band light emission, $I_{B^1\Sigma_g^+ \to X^1\Sigma_u^+}$, is directly proportional to the neutral gas density n_{n,H_2}, plasma density n_e and the molecular excitation rate $\langle v_e \sigma(\epsilon) \rangle$, which allows the measured Lyman band light signal and figure 7 to be used for estimating the ratio of the transient to steady-state electron average energy. The ratio of the transient to steady-state light emission intensity can be expressed as

$$\frac{I_t}{I_{ss}} = \frac{n_{n,t} n_{e,t} [\int \sigma(v) f(v) \, dv]_t}{n_{n,ss} n_{e,ss} [\int \sigma(v) f(v) \, dv]_{ss}} \leqslant \frac{[\int \sigma(v) f(v) \, dv]_t}{[\int \sigma(v) f(v) \, dv]_{ss}}, \quad (3)$$

where $f(v) \, dv$ is the electron velocity distribution function and subscripts t and ss refer to transient and steady state. A similar proportionality can be derived also for Lyman-α intensity $I_{n=2 \to n=1}$ by considering appropriate reactions and cross sections [14]. The inequality in equation (3) follows from two assumptions: (1) the ionization degree of the plasma is small implying constant neutral gas density and (2) the electron density not exceeding the steady-state value during the breakdown transient, i.e. $n_{e,t} \leqslant n_{e,ss}$ (see figure 6).

According to figure 6(*b*) the transient to steady-state intensity ratio for Lyman band emission is 3.3. The normalization of the data in figure 7 allows one to read the *minimum* value of the electron average energy during the breakdown transient at the intersection of the rate curve and horizontal (dashed) line at 3.3 on the vertical scale. It follows for Maxwell–Boltzmann and Druyvesteyn EEDFs that the average minimum electron energies corresponding to the ignition transient, i.e. peak of the light emission, are $\langle \epsilon \rangle_{e,t} \geqslant 13.5$ eV and $\langle \epsilon \rangle_{e,t} \geqslant 10.5$ eV, respectively. These values are somewhat sensitive to the steady-state electron temperature,

$T_e > T_i$ [29]. The curves are normalized to the value at an average electron energy of 7.5 eV corresponding to an electron temperature of 5 eV, i.e. estimated steady-state value, for the Maxwellian distribution. Cross section $\sigma(\epsilon)$ data are taken from [14]. The comparison of the Lyman band VUV signal and the electron saturation current shown in figure 6(*e*) can be considered as evidence of the electron average energy peak. The electron saturation current collected by the probe can be expressed as $I_{e,\text{sat}} = e n_e \langle v_e \rangle A$, where A is the area

Figure 8. Lyman band light signals recorded for (*a*) different powers at 9.3×10^{-3} mbar of gas pressure and (*b*) magnetic field configurations labeled according to the distances measured from the microwave window to the simulated ECR surface at 3000 W of incoming microwave power.

as figure 7 indicates. Altogether, it is concluded that the observed peaks of VUV light emission are clear evidence of the electron average energy peaking during the plasma breakdown process, which is in qualitative agreement with the Langmuir probe data. As shown in figure 7, the rate of ionization grows with the average electron energy more rapidly than the light emission, again in good agreement with the experimental data.

In a stochastic heating process the energy gain W of an individual electron is proportional to the square of the average electric field [26], i.e. $\epsilon \propto E^2$, which holds for both, ECR and collisional off-resonance heating. Thus, the temporal

evolution of the electric field, displayed in figure 6(*a*), suggests that the average electron energy, which is proportional to the temperature of the distribution (e.g. for a Maxwell–Boltzmann distribution $\langle \epsilon \rangle = (3/2)kT_e$) should be expected to decrease to 35–45% of the transient value during the build-up of the plasma density. The steady-state electron temperature of 5 eV yields an estimate of 11–15 eV for the transient value.

Transient electron energies (temperatures) obtained through these independent analytical methods are very similar and they are in reasonable agreement with the Langmuir probe data exhibiting transient behavior. The microwave coupling and VUV-emission data are considerably more reliable than the plasma properties obtained by analyzing the Langmuir probe $I–V$ curves. They provide direct information of the plasma characteristics while the probe curves and their analysis are somewhat sensitive to temporal fluctuations of plasma properties. It was confirmed by modeling that averaging the $I–V$ data over consecutive pulses artificially inflates the electron temperature when the plasma potential fluctuates from pulse-to-pulse even if the slope of the $I–V$ curve and saturation current remain constant. Similar effects are induced if the tail of the EEDF oscillates with time from pulse-to-pulse. Thus, the reliability of the probe data in steady-state plasma conditions can be considered much better than during the ionization cascade when the plasma potential is in a transient phase, as shown in figure 6. VUV-emission spectroscopy and microwave-coupling diagnostics are non-invasive techniques providing 'global' information of the plasma with their sampling power not being restricted to a small localized volume. For the given reasons it is important to estimate the electron temperature during the transient peak by cross-checking the probe data with independent analytical methods as discussed above. This highlights the versatility and temporal resolution of the diagnostic setup which, to our knowledge, is one of the most sophisticated ones ever used for studying transient effects of hydrogen plasmas in 2.45 GHz microwave discharges.

In order to demonstrate that the interpretation of the data is valid for a wide range of experimental conditions we present Lyman band light signals recorded with different microwave powers in figure 8(*a*) and magnetic field configurations in figure 8(*b*). The magnetic field configurations have been labeled according to the distance measured from the microwave window to the (simulated) resonance surface. In all cases the VUV signal exhibits a ~10 μs transient peak indicating higher electron energy at the beginning of the discharge pulse. The data are averaged over 128 consecutive pulses. Interestingly, the breakdown transient peak is also observed with the magnetic field configuration for which there is no resonance in the plasma chamber, i.e. $B < 87.5$ mT. This highlights that the nature of the transient is independent of the exact energy transfer mechanism from the microwave to the electrons, which supports the assumption made for the analysis of the reflected/incident power data.

Finally, the data in figure 9 establish a saturation time for the plasma parameters. The saturation of the Lyman-α and Lyman band emission signals is reached in about 400–500 μs. It is worth noting that the plasma parameters obtained
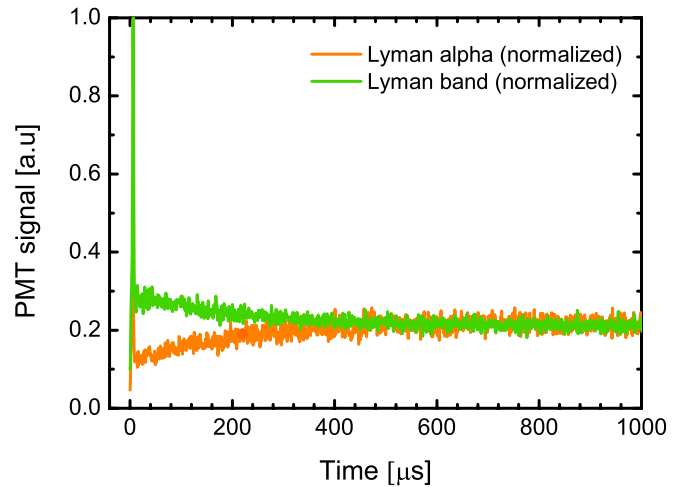
Figure 9. Lyman-α and Lyman band VUV signals showing a typical saturation time of ~ 400 μs to reach the steady-state plasma condition.

with the Langmuir probe, i.e. plasma potential and electron temperature and density, reach their steady-state values much faster (typically in 20–50 μs). The saturation behavior of the VUV signals is therefore attributed to the evolving atomic to molecular H/H_2 species fraction. This conclusion is supported by the fact that the VUV signal saturation time is similar to typical saturation time of the $H^+/H_2^+/H_3^+$ species fraction of the ion beam extracted from 2.45 GHz ion sources measured, e.g., by Xu *et al* [11].

4. Conclusions

It is concluded that our data support the following qualitative model for the plasma breakdown: initially the plasma density is low allowing the average microwave electric field in the plasma chamber to build up. Under such conditions electrons are heated efficiently and the average energy of their population reaches values exceeding the saturation value. Exponentially increasing plasma density causes the average electric field and electron energy to decrease until the diffusive loss rate of electrons matches the ionization rate of the neutral H_2-gas. The VUV light emission depends strongly on the electron average energy and, therefore, exhibits a strong transient peak associated with the plasma breakdown. The ionization rate (dn_e/dt) is proportional to the neutral gas density and electron average energy, i.e. the plasma density increases almost exponentially until the steady state is reached. The 10 μs ignition transient corresponds to the progress of the ionization cascade. The given interpretation of this time scale is supported by the calculated average collision time of 100–500 ns for 15 eV electrons in the neutral gas pressure range corresponding to our experimental conditions (cross section data from [14]). The saturation of the probe data is achieved in 20–50 μs, which corresponds to the temporal scale of the ion motion ($T_i < 1$ eV) at the relevant length scale, i.e. chamber dimension of ∼0.1 m. Finally, the 400–500 μs saturation time of the atomic and molecular VUV signals corresponds to the temporal evolution of the species fraction. The model

is similar to that suggested for high-frequency ECR ion sources [5]. However, this study provides significantly more data, both direct and indirect, supporting the interpretation and extends the validity of the model from high-frequency minimum-*B* ECR ion sources to 2.45 GHz microwave plasma discharges where the temporal evolution of plasma parameters is significantly faster due to higher neutral gas pressure. The experiments indicate that maintaining the electron temperature at the transient level could enhance the ionization rate and improve the efficiency of 2.45 GHz microwave ion sources.

Acknowledgments

References

[1] Gammino S, Celona L, Ciavola G, Maimone F and Mascali D 2010 *Rev. Sci. Instrum.* **81** 02B313

[2] Pelletier J and Anders A 2005 *IEEE Trans. Plasma Sci.* **33** 1944–59

[3] Tarvainen O, Ropponen T, Toivanen V, Ärje J and Koivisto H 2009 *Plasma Sources Sci. Technol.* **18** 035018

[4] Bäcker H, Bradley J W, Kelly P J and Arnell R D 2001 *J. Phys. D: Appl. Phys.* **34** 2709–14

[5] Ropponen T *et al* 2011 *Plasma Sources Sci. Technol.* **20** 055007

[6] Lyneis C, Benitez J, Leitner D, Noland J, Strohmeier M, Koivisto H and Tarvainen O 2010 Characterization of the microwave coupling to the plasma chamber of the LBL ECR ion source *Proc. ECRIS 2010 (Grenoble, France)* pp 162–4

[7] Celona L, Gammino S, Maimone F, Mascali D, Gambino N, Miracoli R and Ciavola G 2011 *Eur. Phys. J.* D **61** 107

[8] Celona L, Gammino S, Ciavola G, Maimone F and Mascali D 2011 *Rev. Sci. Instrum.* **81** 02A333

[9] Ropponen T, Tarvainen O, Toivanen V, Peura P, Jones P, Kalvas T, Koivisto H, Noland J and Leitner D 2010 *Rev. Sci. Instrum.* **81** 02A302

[10] Luggenhölscher D, Czarnetzki U and Dobele H 2000 Investigations on electric field distributions in a microwave discharge in hydrogen. *Proc. 53rd Annual Gaseous Electronics Conf. (Houston, TX, 24–27 October 2000)* Abstract ETP.070

[11] Xu R, Zhao J, Peng S, Yuan Z, Song Z, Yu J and Guo Z 2008 *Rev. Sci. Instrum.* **79** 02B713

[12] Miracoli R, Gammino S, Celona L, Castro G, Mascali D, Gobin R, Delferrier O, Adroit G, Senee F and Ciavola G 2012 *Rev. Sci. Instrum.* **83** 056109

[13] Rousseau A, Teboul E, Lang N, Hannemann M and Röpcke J 2012 *J. Appl. Phys.* **92** 3463–71

[14] Yoon J, Song M, Han J, Hwang S, Chang W and Lee B 2008 *J. Phys. Chem. Ref. Data* **37** 913–31

[15] Cortázar O D, Megía-Macías A and Vizcaíno-de Julián A 2012 *Rev. Sci. Instrum.* **83** 103302

[16] Chen F, Evans J and Arnush D 2002 *Phys. Plasmas* **9** 1449–55

[17] Boswell R 1988 *Plasma Phys. Control. Fusion* **26** 1147–62

[18] Ajello J, Srivastava S and Yung Y 1982 *Phys. Rev. A* **25** 2485–98

[19] Merlino R L 2007 *Am. J. Phys.* **75** 1078–85

[20] Tuszewski M and Tobin J A 1996 *Plasma Sources Sci. Technol.* **5** 640–7

[21] Chen F F 1965 *Plasma Diagnostics Techniques* ed R H Huddlestone and S L Leonard (New York: Academic)

[22] Sherman J, Figueroa T, Hansborough L, Kerstiens D, Shneider J, Smith H Jr, Stettler M, Stevens R Jr, Thuot M, Warren D and Zaugg T 2002 *Rev. Sci. Instrum.* **73** 917–21

[23] Meeker D 2010 *Finite Element Method Magnetics* version 4.2, www.femm.info

[24] Cortázar O D, Megía-Macías A and Vizcaíno-de Julián A 2012 *IEEE Trans. Plasma Sci.* **40** 3409–19

[25] J C Slater 1963 *Microwave Electronics* (New York: Van Nostrand) pp 51–76

[26] Williamson M C, Lichtenberg A J and Lieberman M A 1992 *J. Appl. Phys.* **72** 3924–33

[27] Goto M, Sawada K and Fujimoto T 2002 *Phys. Plasmas* **9** 4316–24

[28] Toivanen V, Tarvainen O, Lyneis C, Kauppinen J, Komppula J and Koivisto H 2012 *Rev. Sci. Instrum.* **83** 02A306

[29] Druyvesteyn M and Penning F 1940 *Rev. Mod. Phys.* **12** 87–174